

## Article

# Influence of Superlattice Structure on V-Defect Distribution, External Quantum Efficiency and Electroluminescence for Red InGaN Based $\mu$ LEDs on Silicon

Jacob Ewing <sup>1,\*</sup>, Cheyenne Lynsky <sup>1</sup>, Jiaao Zhang <sup>1</sup>, Pavel Shapturenka <sup>2</sup>, Matthew Wong <sup>1</sup>, Jordan Smith <sup>1</sup>, Michael Iza <sup>1</sup>, James S. Speck <sup>1</sup> and Stephen P. DenBaars <sup>1,3</sup>

<sup>1</sup> Materials Department, University of California, Santa Barbara, CA 93106, USA

<sup>2</sup> Chemical Engineering Department, University of California, Santa Barbara, CA 93106, USA

<sup>3</sup> Department of Electrical and Computer Engineering, University of California, Santa Barbara, CA 93106, USA

\* Correspondence: ewing@ucsb.edu

**Abstract:** Achieving high quantum efficiency in long-wavelength LEDs has posed a significant challenge to the solid-state lighting and display industries. In this article, we use V-defect engineering as a technique to achieve higher efficiencies in red InGaN LEDs on (111) Si through lateral injection. We investigate the effects of superlattice structure on the V-defect distribution, the electroluminescence properties, and the external quantum efficiency. Increasing the relative thickness of In in the InGaN/GaN superlattice and the total superlattice thickness correlate with a reduction of active region defects and increased external quantum efficiencies. The highest measured on-chip EQE was 0.15% and based on Monte-Carlo ray tracing simulations for light extraction we project this would correspond to a flip-chip EQE of ~2.5%.

**Keywords:** red InGaN; microLEDs; v-defect; superlattice



**Citation:** Ewing, J.; Lynsky, C.; Zhang, J.; Shapturenka, P.; Wong, M.; Smith, J.; Iza, M.; Speck, J.S.; DenBaars, S.P. Influence of Superlattice Structure on V-Defect Distribution, External Quantum Efficiency and Electroluminescence for Red InGaN Based  $\mu$ LEDs on Silicon. *Crystals* **2022**, *12*, 1216. <https://doi.org/10.3390/cryst12091216>

Academic Editor: Paul J. Simmonds

Received: 20 July 2022

Accepted: 26 August 2022

Published: 28 August 2022

**Publisher's Note:** MDPI stays neutral with regard to jurisdictional claims in published maps and institutional affiliations.



**Copyright:** © 2022 by the authors. Licensee MDPI, Basel, Switzerland. This article is an open access article distributed under the terms and conditions of the Creative Commons Attribution (CC BY) license (<https://creativecommons.org/licenses/by/4.0/>).

## 1. Introduction

Long-wavelength LEDs have become an increasingly important area of research in the LED industry due to the large number of lighting and display applications. For display applications, there's increasing interest in microLEDs ( $\mu$ LEDs) which show tremendous promise in providing highly efficient, self-emissive light sources, with high fidelity and brightness [1]. While blue InGaN  $\mu$ LEDs show high efficiency and size-independent properties due to numerous advances including side-wall passivation [2], long-wavelength InGaN  $\mu$ LEDs (especially red) have proved more difficult to realize high efficiencies and size independent properties. This is due in part to the difficulties of achieving high In% in the InGaN QWs during metal-organic chemical vapor deposition (MOCVD) growth. Achieving high In% requires lower growth temperatures which tend to decrease crystal quality forming unwanted defects and stacking faults which become sites for non-radiative recombination [3]. Additionally, since In is a larger atom than Ga, substituting In on Ga sites in the wurtzite crystalline lattice generates compressive stress in the InGaN layers. This stress further increases the chance of forming unwanted defects in the active region as well as increasing piezoelectric polarization which decreases the electron and hole wavefunction overlap. Piezoelectric polarization along with alloy fluctuations have been shown to have a significant impact on carrier transport through long-wavelength InGaN devices [4,5]. The result of all these factors markedly decreases the electrical efficiency of InGaN red LEDs compared to blue or green.

Many approaches have been employed to combat the challenges facing long-wavelength InGaN LEDs. These include a variety of strain-relaxed methods which seek to use epitaxial and strain engineering to reduce the compressive stress in the InGaN layers and thus reduce the piezoelectric effects and In desorption during growth. These methods include

porous GaN [6], InGaNOS pseudo-substrates [7], and strain relaxed templates [8]. Strain relaxed techniques enable higher growth temperatures in the active region due to decreased ‘compositional pulling’ during quantum well growth. These higher growth temperatures may also reduce the concentration of impurities and native defects and the reduced strain in the quantum well can decrease the Quantum Confined Stark Effect (QCSE) increasing the electron and hole wavefunction overlap. The challenge with strain relaxed methods is that very often, in the attempt create strain relaxation in the base layers, the morphology of the LED is compromised, leading to inconsistent growth results and generation of an unacceptably high density of threading dislocations. Nevertheless, strain-relaxed methods have successfully demonstrated many impressive results in red InGaN LEDs.

Another approach to long-wavelength InGaN LEDs is the use of lateral injection of the quantum wells [9]. This method seeks to find a balance between the key challenges facing red InGaN and boost the device performance through volumetric injection of the quantum wells, generally achieved through strategic use of naturally occurring V-shaped inverted hexagonal pyramidal (10–11) defects (V-defects). In vertically injected LEDs, it’s well known that only the first couple quantum wells on the p-side are injected with sufficient holes to produce substantial light output. Quan et al. showed that V-defects both screen threading dislocations that would otherwise be a source of non-radiative recombination and provide holes energetically favorable pathways through the semi-polar sidewalls of the V-defects that enable injection into deeper wells and significantly reduce the forward voltage of green through red LEDs [10,11]. The deeper injection is useful for both increasing peak efficiency and mitigating efficiency droop. V-defect methods still face all the challenges that other InGaN red LEDs face such as QCSE, lattice strain, active region defects, and strain buildup, but if all these can be minimized and an optimal V-defect structure can be demonstrated with sufficient defect density, V-defect methods represent the highest wall-plug efficiency of any technique for growing red InGaN LEDs [12,13].

V-defects nucleate on threading dislocations (TD) formed deep in the 3D-GaN structure [14]. Threading dislocation density (TDD) is known to vary based on substrates and growth conditions and is generally higher on Si compared to patterned sapphire substrates (PSS). For many LED structures the increased TDD on Si is a detriment but for V-defect engineered LEDs it can be an asset if the threading dislocations are successfully nucleated into V-defects at the appropriate place in the epitaxial stack. Tao et al. and Jiang et al. have shown that an InGaN/GaN superlattice can be an effective way to nucleate V-defects before the active region growth and may provide further benefits for red InGaN LED performance [15,16]. Other papers have investigated low-temperature GaN as another mechanism for nucleating V-defects [17]. Some researchers have argued that a uniform distribution of large V-defects nucleated in the superlattice, or comparable nucleation layer, is the optimal structure for high performing long-wavelength LEDs [18]. In this paper we investigate a few possible superlattice structures and analyze the V-defect distribution using SEM backscatter imaging combined with image processing techniques. The growth conditions are correlated with V-defect distribution, external quantum efficiency, size-dependent properties of  $\mu$ LEDs and the electroluminescence spectra.

## 2. Methods

### 2.1. MOCVD Growth

The red LEDs were grown via MOCVD on commercial GaN-on-Si templates from Enkris Semiconductor. The template structure was 1 mm (111) Si, a buffer layer < 800 nm, 2  $\mu$ m UID GaN, and 2  $\mu$ m n-GaN with a [Si] >  $3 \times 10^{18}$  cm<sup>-3</sup>. The (002) and (102) rocking curve widths of the templates were 355 and 546 arcseconds, respectively. The 6-inch Si wafers were diced into 13  $\times$  13 mm<sup>2</sup> squares which were used for regrowth of LEDs and subsequent processing. The regrown LED structure is shown in Figure 1. Growth was initiated with a 500 nm n-GaN with [Si] =  $5 \times 10^{18}$ , followed by a 30-period GaN/InGaN (~5% In) superlattice (SL) also with [Si] =  $5 \times 10^{18}$ . 3 different samples were grown, each with a different InGaN thickness. The GaN thickness was kept constant at 5 nm and the

InGaN thickness was 2.5 nm, 3.75 nm, and 5 nm for Samples A, B, and C, respectively. A 2-nm UID GaN spacer was grown immediately before the 7 MQWs. The 2.5 nm InGaN QWs were all grown at susceptor temperature of 762 °C followed immediately by a 30% Al, AlGaIn cap grown at the same temperature. The AlGaIn cap is used to keep In inside the QW and prevent it from desorbing during subsequent higher temperature GaN barrier growth. After the AlGaIn cap, the temperature was increased by 102 °C for the low-temperature GaN barrier and then increased an additional 55 °C for the high-temperature GaN barrier. The GaN barriers were grown at a reduced growth rate and higher temperature to recover some of the crystal quality in the active region. After the MQW region, a 10 nm p-AlGaIn electron blocking layer (EBL) was grown with  $[Mg] = 9 \times 10^{19} \text{ cm}^{-3}$  and 75 nm p-GaN with  $[Mg] = 5 \times 10^{19} \text{ cm}^{-3}$ . Finally, a 10 nm p+ GaN layer was grown to improve the ohmic contacts.

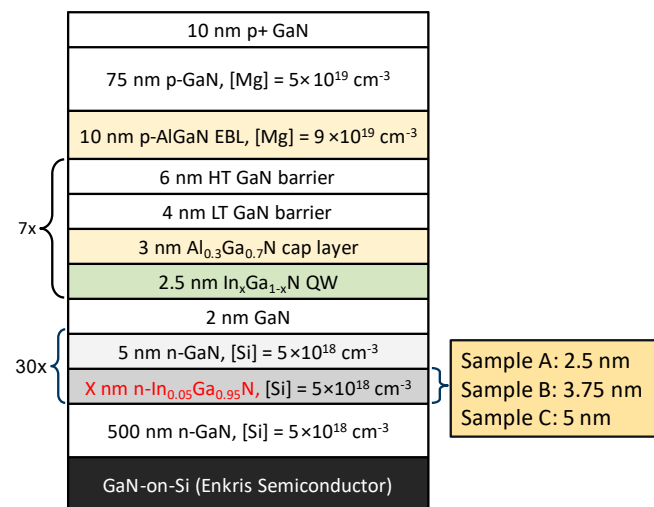


**Figure 1.** Epitaxial structure for GaN-on-Si red LEDs.

## 2.2. V-Defect Distribution

The V-defect distribution was characterized by backscatter scanning electron microscope (BS-SEM) images on as-grown epi. Backscatter images were used because they provide simpler contrast than secondary electron SEM which made image processing easier. SEM images were taken at 15,000 $\times$  magnification with a spot size of 4 nm and a beam voltage of 4 keV. Image processing was done with python 3, utilizing the Numpy and Scikit-image libraries and matplotlib for plotting. The images were thresholded to isolate V-defects, then polygons were drawn around the edges of each v-pit. The polygon dimensions were used to estimate average v-pit sizes. The results of 4 images taken near the center of each sample were plotted in histograms to estimate v-pit size distribution. Figure 2 shows an example of a backscatter SEM image showing V-defects and a thresholded image with polygons drawn around each V-defect. From this, histograms can be generated giving the V-defect distribution.

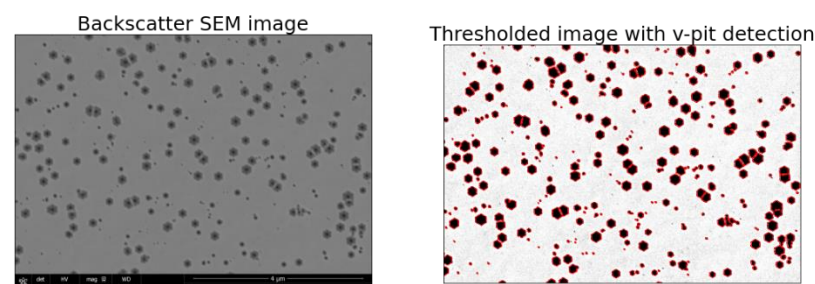


**Figure 2.** Backscatter SEM image showing V-defects before and after image processing.

### 2.3. Device Processing

Fabrication followed a standard  $\mu$ LED process developed at UCSB with  $\mu$ LED sizes ranging from 5  $\mu\text{m}$ –100  $\mu\text{m}$  [19,20]. 110 nm of indium-tin-oxide (ITO) was deposited over the p-GaN to help with current spreading. Mesas were etched using a  $\text{CH}_3/\text{H}_2/\text{Ar}$  reactive ion etch (RIE) for ITO and a  $\text{SiCl}_4$  RIE for GaN. The etch depth of the GaN was  $\sim$ 700 nm. A  $\text{SiO}_2/\text{Ta}_2\text{O}_5/\text{Al}_2\text{O}_3$  omnidirectional reflector (ODR) was deposited via ion beam deposition (IBD) under the contacts. Atomic layer deposition (ALD) was used to deposit a 25 nm  $\text{SiO}_2$  layer for sidewall passivation. 500/100/500 nm Al/Ni/Au contacts were deposited via electron beam deposition.

### 2.4. Characterization

Electroluminescence (EL) characteristics were measured using an on-chip topside collecting 6-inch diameter integrating sphere. The integrating sphere setup uses a single open port to collect light at an angle of  $\sim$ 180 degrees. The sphere was calibrated using a standard light source from Ocean Insight. The light collected from the integrating sphere was sent through an optical fiber to a monochromator and the light was analyzed with a CCD detector. EQE measurements were taken on-chip with an absorbing Si substrate so the expected light extraction for these LEDs is significantly lower than comparable LEDs on sapphire or another transparent substrate. The CCD detector has a limited wavelength range so to study the entire spectra from 400–700 nm an Ocean Optics spectrometer was used to measure the EL at selected current densities.

To estimate an accurate IQE and project a flip-chip EQE without an absorbing substrate, Monte Carlo ray tracing simulations were performed using Synopsys LightTools. The simulated structure replicates an LED mesa with ITO contacts, and an ODR with a uniform emission box in the active region of the LightTools LED. This structure was placed on an absorbing Si substrate and the Monte Carlo simulation generated 1,000,000 rays from a 100-nm volume source at 620 nm and 35 nm FWHM. Further calculations simulated the flip-chip configuration with an inverted mesa, a 3  $\mu\text{m}$  90% reflective silver layer, and a Lambertian-scattering surface with 50/50 first-pass transmission probability on the top side of the mesa. The mesa size was 20  $\mu\text{m}$  but it was demonstrated that the light extraction efficiency (LEE) did not vary significantly for different mesa sizes. The calculated LEE for a red  $\mu$ LED on Si was 4.97%. This compared with 85% LEE from an expected flip-chip structure, means that the measured on-chip EQE is substantially lower than the projected flip-chip EQE. Both the measured on-chip EQE and the projected flip-chip EQEs have been plotted in the Results section.

## 3. Results

### 3.1. V-Pit Distribution

Figure 3 shows the V-defect distribution for samples A, B, and C. The GaN-on-Si substrates are diced from the same 6 in wafer so the TDD should be equivalent for all samples. Then, we expect that the differences in distribution arise from nucleation conditions in the superlattice where V-defects form around threading dislocations as well as the growth conditions in the active region, which affect the formation of small, generally unwanted V-defects. There is a clear bimodal distribution of V-defects for all samples. This likely represents some fraction of the v-defects that nucleate in the superlattice and a fraction that nucleate higher in the structure, probably in the latter part of the MQW region.

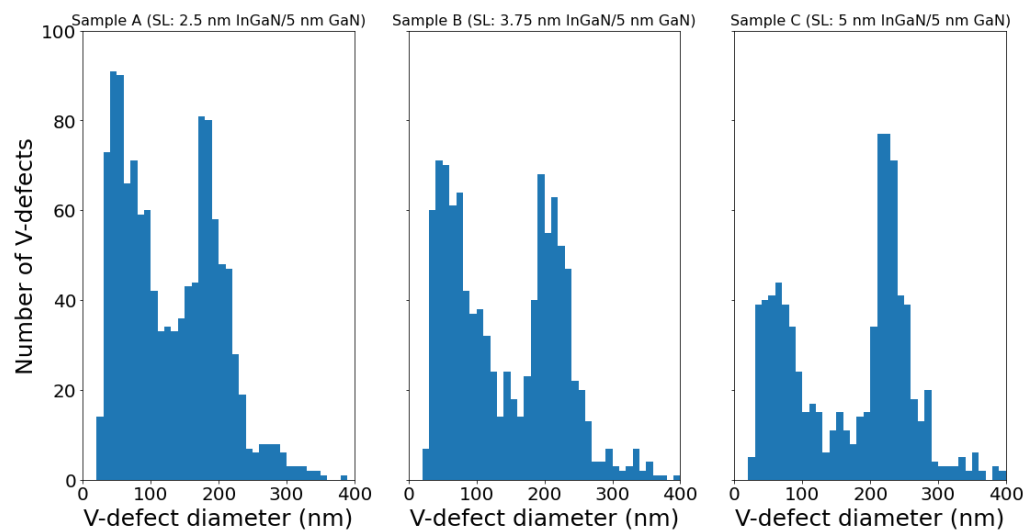


**Figure 3.** V-defect distribution for samples A, B, and C.

From Figure 3 we see that sample C with thicker InGaN has a higher fraction of large V-defects to smaller V-defects compared to Sample B and especially to Sample A. Qi et al. have argued that larger V-defects, namely those that form in the superlattice, are more beneficial to device performance and do not promote leakage like smaller v-pits that form in the MQWs [21]. While it's generally agreed that large V-defects form around threading dislocations generated deep in the 3D-GaN and nucleate when growth conditions such as temperature, growth rate, and V/III ratio are favorable for nucleation, it's less obvious where and why these smaller V-defects form. While it's likely that many still form around threading dislocations from the 3D-GaN some researchers have argued that they may also form around basal plane stacking faults [22]. These basal plane stacking faults might be generated in the InGaN QWs or the AlGaIn capping layers. The formation of basal plane stacking faults and small V-defects is an area that requires much more research but it's not unreasonable to assume that preparation layers such as GaN/InGaN superlattices could affect the strain in the QWs and the formation of a variety of defects higher in the structure.

Table 1 shows some basic statistics regarding distribution of V-defects from the BS-SEM image analysis. The V-defect density is calculated directly from the SEM images. The percent of V-defects formed in the superlattice is estimated based off the geometry of the crystallographic defects and the depth of the structure. For the purposes of this paper, the 'large V-defects' and 'V-defects forming in the SL' are used synonymously. Interestingly, despite the different nucleation conditions in the superlattice samples A, B, and C all have very similar densities of large V-defects. It's the small V-defects that likely form in the active region that are affected by the superlattice growth conditions. The difference in average diameter is partly a reflection of fewer small V-defects in samples B and C but is also reflective of the total superlattice thickness being greater for Samples B and C. This effect can also be seen in the histograms in Figure 3.

**Table 1.** Statistics on v-pit distribution for 3 LEDs with different SL structures.

Sample	Density of V-Defects	% Formed in SL	Density of V-Defects Formed in SL	Average Diameter (nm)
A	$6.38 \times 10^8$	47.4%	$3.02 \times 10^8$	129.1
B	$5.39 \times 10^8$	48.5%	$2.61 \times 10^8$	142.9
C	$4.35 \times 10^8$	58.2%	$2.53 \times 10^8$	171.6

### 3.2. Electroluminescence and External Quantum Efficiency

A common problem discussed by researchers looking at red InGaIn is the existence of parasitic emission at undesired wavelengths. Generally, this is blue emission, and much

research has surrounded its origin and mitigation [23–25]. Unfortunately, there does not seem to be consensus about the origin or the nature of these blue peaks which may indicate that it's a complicated problem with a variety of potential sources and mitigation strategies. The LEDs fabricated in this paper did display blue emission but only at reasonably high current densities, which is not always the trend observed. Figure 4a shows the emission spectra taken on-chip with a spectrometer at 20, 50, 100, and 300 A/cm<sup>2</sup> from an 80 μm LED on Sample C. At 20 A/cm<sup>2</sup> there is essentially no blue emission and there is still very little at 50 A/cm<sup>2</sup>. By 100 A/cm<sup>2</sup> there is appreciable blue emission and the LED looks visually pink. By 300 A/cm<sup>2</sup> the blue emission is so strong that it's almost equal in intensity to the main red emission peak. For some devices, especially on sample A which has the most intense blue emission, the intensity of the blue peak exceeded that of the red peak at 300 A/cm<sup>2</sup>. Whatever, the source of the blue emission it seems to be a diode acting in parallel with a higher turn-on voltage.

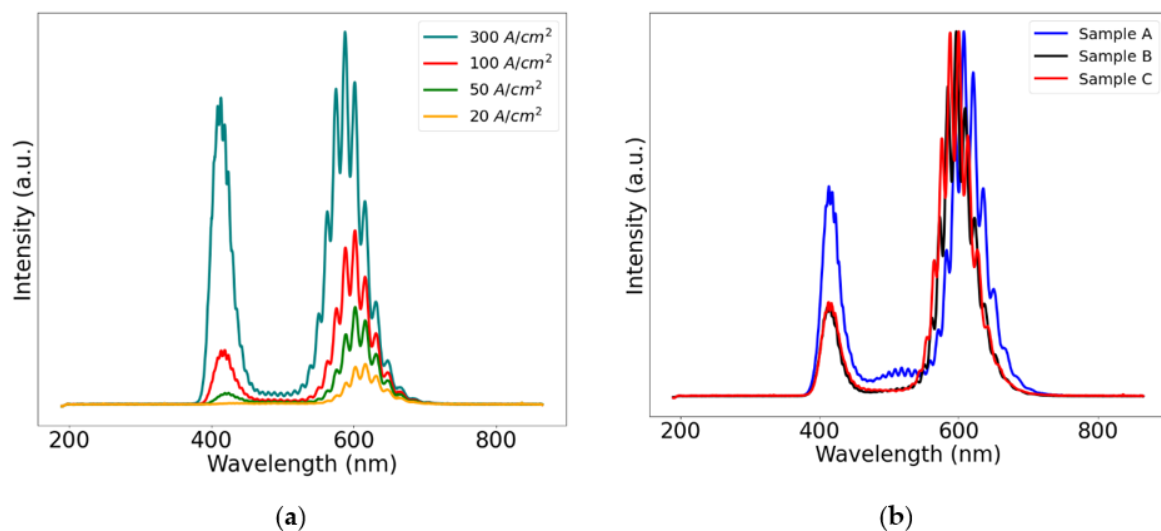


**Figure 4.** (a) Blue emission as a function of current density for an 80 μm LED from Sample C. The Fabry-Perot fringes are due to the EL spectra being measured on-chip with a Si substrate (b) EL spectra at 100 A/cm<sup>2</sup> showing parasitic blue emission with red emission for samples A, B, and C.

Figure 4b shows a comparison between the 3 samples at 100 A/cm<sup>2</sup>. Sample A which has the highest number of small v-defects also displays the most intense blue emission. Samples B and C showed very similar blue emission although there was a bit of variability device to device on the same chip.

Figure 5 shows the EQE measurements for each sample with devices ranging from 100 μm down to 5 μm. On the left-hand axis is the measured on-chip EQE collected from the topside integrating sphere. The right-hand axis is the 'Projected Flip-Chip (FC) EQE' based on the Monte-Carlo LightTools simulations discussed earlier. This accounts for the 5% LEE on silicon and projects an efficiency if the substrate was removed and the flip-chip architecture had a LEE of 85% (also based on Monte-Carlo LightTools simulations). The assumption then is that if these LEDs went through flip-chip processing and substrate removal the efficiency would be similar to the EQE on the right-hand axis of the plots in Figure 5. It should be noted that the CCD detector used to collect this data only collects light in a limited window ~540–680 nm so any blue emission does not factor into the total efficiency. Therefore, EQEs presented are the EQEs of *red emission* only. Additionally, the blue emission is relatively low in the current density range being measured.

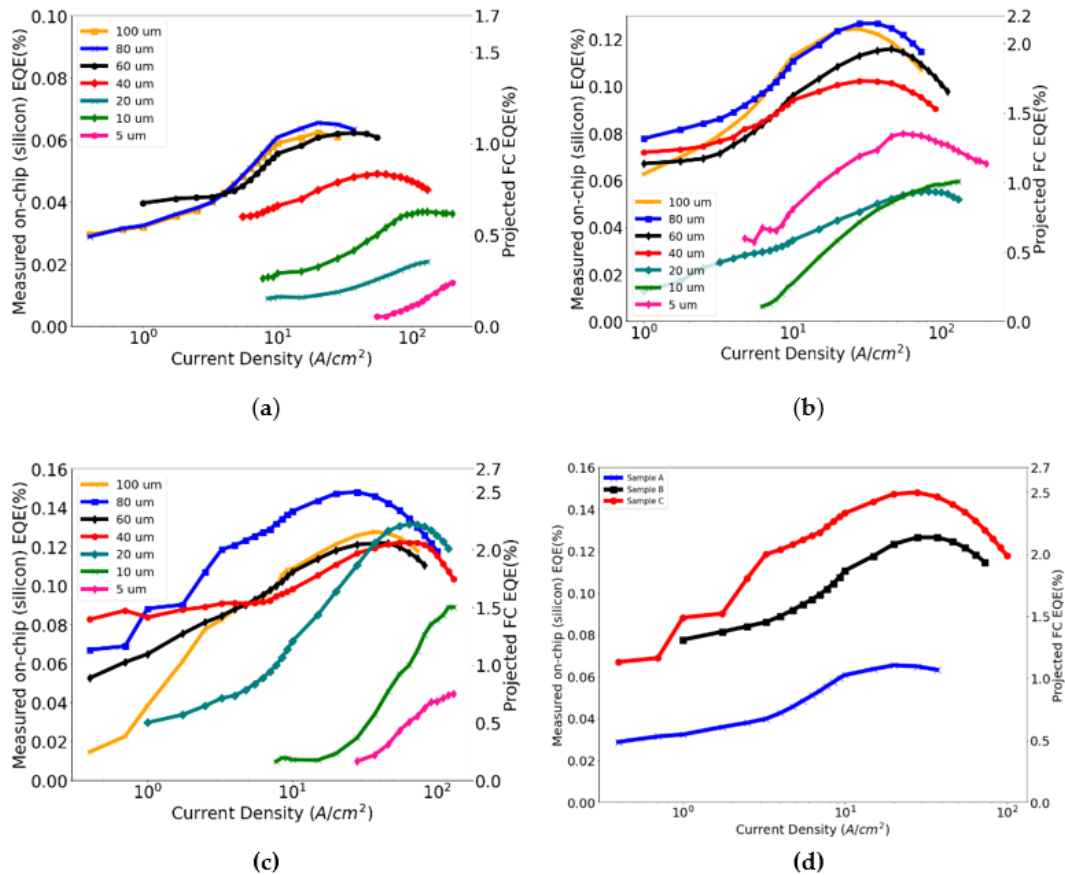


**Figure 5.** EQE plots for 5–100  $\mu\text{m}$  microLEDs for samples (a), (b), and (c), respectively (d) EQE comparison for highest EQE device from each chip (80  $\mu\text{m}$ ).

The peak EQE is the lowest for sample A and increases for sample B still further for sample C. The projected efficiency for the best device on sample C is  $\sim 2.5\%$ . There are also trends in the size-dependence. Sample A shows size-independence only for 60–100  $\mu\text{m}$  devices and the efficiency steadily falls off for 5–40  $\mu\text{m}$  LEDs. Sample B displays nearly twice the peak efficiency for the 80 and 100  $\mu\text{m}$  LEDs compared to sample A. 40 and 60  $\mu\text{m}$  LEDs still display relatively high efficiency. For  $\mu\text{LEDs} \leq 20 \mu\text{m}$ , the peak efficiency shifts to higher current densities and the efficiency is only  $\frac{1}{2}$  to  $\frac{1}{3}$  of the peak EQE for the larger devices. Finally, Sample C, which has the most favorable V-defect distribution, showed the highest peak efficiency and nearly size independent EQE from 20–100  $\mu\text{m}$ . Only for 5 and 10  $\mu\text{m}$  was the efficiency reduced and the peak EQE shifted to  $>100 \text{ A/cm}^2$ . Figure 5d shows a direct comparison between the three samples for 80  $\mu\text{m}$  LEDs on each chip.

Figure 6a shows the wavelength dependence as a function of current density for a couple devices from each sample. For each sample the low current density wavelength was 630–640 nm and dropped to  $\sim 600$ –610 nm at  $100 \text{ A/cm}^2$ . Figure 6b shows the electroluminescence spectra at low current densities for the 80  $\mu\text{m}$  LED on sample C which had a projected EQE of  $\sim 2.5\%$ . The shift in emission wavelength is an indication that these LEDs are realizing a sufficiently high carrier density to screen some of the piezoelectric field. The absence of the Fabry-Perot fringes is due to these spectra being taken using an integration sphere which randomizes the direction of the light being emitted.

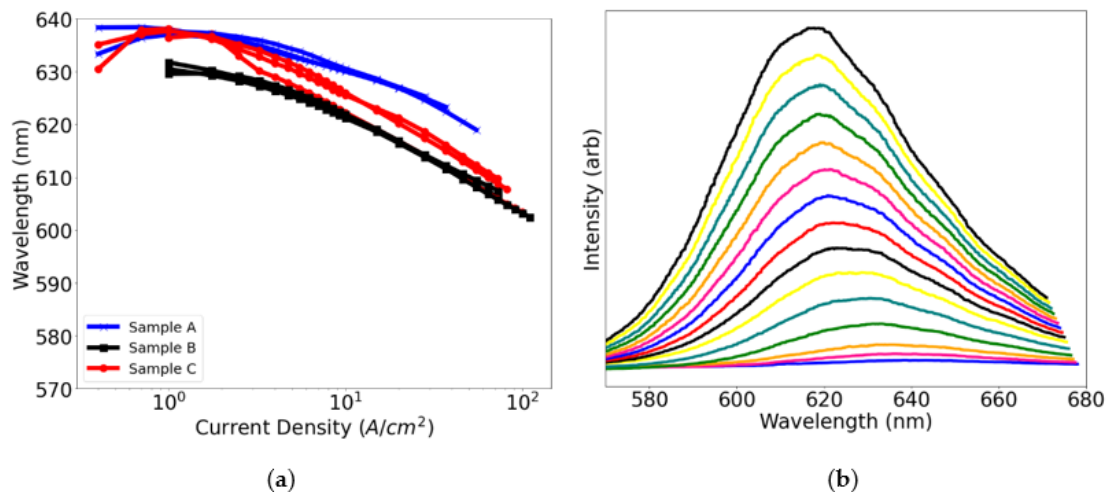


**Figure 6.** Emission profile of red  $\mu$ LEDs on Si (a) Wavelength vs. current density plots for two  $\mu$ LEDs from each sample (b) Spectra at various current densities (0.4–10 A/cm<sup>2</sup>) for an 80  $\mu$ m LED from sample C. Peak emission shifts from 640 nm to 620 nm.

#### 4. Discussion

Superlattices in InGaN LEDs serve many different purposes, from improving carrier dynamics, to incorporating extrinsic impurities, to nucleating v-defects. For yellow and red InGaN there are still many open questions about exactly what role the superlattice plays in increasing performance. Some researchers have argued that SLs, especially those with thick InGaN and high In content, can increase In incorporation in the QWs making it easier to achieve long-wavelength emission [15]. In this article, we see clear evidence that the superlattices affect V-defect formation and size but did not see a noticeable wavelength shift indicating higher In content with thicker InGaN. Some researchers do see significant affect in In incorporation with changed V-defect structure [26], however in our experiments we saw mostly a reduction in ‘small’ V-defects whereas it’s most likely the large V-defects (those where hole injection is increased) that would affect emission wavelength. It’s difficult to pin down the exact mechanisms by which higher EQEs are achieved but it seems clear that Shockley-Read-Hall (SRH) centers play a big role. In this study we saw improved EQE when we reduced the small V-defects forming in the active region which very likely were centers for SRH. In general, achieving high crystal quality in the MQW region remains one of the key challenges for red InGaN and future work needs to focus on strategic use of V-defects to achieve the highest crystal quality possible in the QWs.

Another key challenge is the mitigation of parasitic blue emission which has been shown to occur from a variety of different sources including superlattice emission, In depletion and/or clustering around defects, and QWs grown on the semi-polar sidewalls of v-pits. More work is required to identify the exact mechanism in the LEDs described here but we do see a possible trend with blue emission being correlated with active region defects. The origin of the parasitic blue emission in red InGaN LEDs remains a topic of on-going study in our group.

A plausible explanation for the EQE trends that relates the v-pit distributions starts with the idea that small V-defects, forming on threads or around stacking faults, are centers for SRH recombination. A significant part of the ‘green gap’ and the difficulties in attaining high EQE in long-wavelength InGaN, stems from SRH. If the small V-defects are centers for SRH, then finding preparation layers that help minimize those defects would result in higher EQEs which is what we observed in Samples A, B, and C in this paper.

Another very interesting trend was that the samples with fewer small V-defects, especially sample C, appear to also display more size independent properties for  $\mu$ LEDs. Size trends in  $\mu$ LEDs are also known to, at least in part, be the result of SRH occurring through sidewall defects which become a larger fraction of the total recombination due to

the increased perimeter to volume ratio of small  $\mu$ LEDs [26] Higher SRH in small  $\mu$ LEDs is likely responsible for both the reduced EQE and higher current density required to reach peak EQE in the 5–20  $\mu\text{m}$  devices. This is further supported by the EQE behavior of the small LEDs which have very low efficiency and do not droop, typical behavior of SRH or trap-assisted Auger recombination (TAAR) dominated LEDs [27]. Perhaps the existence of V-defects (especially those initiated in the QWs) on the mesa sidewalls become ‘super SRH centers’ and further degrade efficiency. If sample C had less of these ‘super SRH centers’, then it might display more size-independent properties than the other samples as borne out by the data.

## 5. Conclusions

In this article we grew samples with different superlattice structures in red InGaN LEDs on (111) Si and correlated those growth conditions with v-defect size distribution, electroluminescence properties and external quantum efficiencies. We saw that thicker superlattices with thicker InGaN in the superlattice were effective in reducing the number of small v-defects nucleating in the active region and this was correlated with higher EQEs, more size-independent efficiencies for  $\mu$ LEDs, and reduced parasitic blue emission. We discussed the possibility that unwanted v-defects in the active region may become SRH centers and the existence of these SRH centers may explain the EQE trends and size-dependent efficiencies in the  $\mu$ LEDs. Finally, we discussed how preparation layers may influence the crystal quality of red InGaN QWs. Future work should seek to understand these mechanisms both theoretically and experimentally.

**Author Contributions:** Conceptualization, J.E. and C.L.; methodology, J.E. and C.L.; software, J.E., J.S. and P.S.; validation, J.E.; formal analysis, J.E. and P.S.; investigation, J.E. and J.Z.; resources, M.I., M.W., J.S.S. and S.P.D.; data curation, J.E. and J.Z.; writing—original draft preparation, J.E.; writing—review and editing, J.E. and S.P.D.; visualization, J.E.; supervision, M.I., S.P.D. and J.S.S.; project administration, S.P.D.; funding acquisition, S.P.D. All authors have read and agreed to the published version of the manuscript.

**Funding:** This material is supported in part by the National Science Foundation Graduate Research Fellowship Program. Any opinions, findings, and conclusions or recommendations expressed in this material are those of the author(s) and do not necessarily reflect the views of the National Science Foundation. This work was supported by Applied Materials, Inc. in Santa Clara, California and the Solid-State Lighting and Energy Electronics Center (SSLEEC). Additional support was provided by DOE EERE (BENEFIT Program) Award number DE-EE0009691.

**Data Availability Statement:** Relevant data used for this study is given in the paper.

**Acknowledgments:** The authors acknowledge the use of the research facilities within the California NanoSystems Institute, supported by the University of California, Santa Barbara, and the University of California, Office of the President. A portion of this work was performed in the UCSB Nanofabrication Facility, an open access laboratory.

**Conflicts of Interest:** The authors declare no conflict of interest. The funders had no role in the design of the study; in the collection, analyses, or interpretation of data; in the writing of the manuscript; or in the decision to publish the results.

## References

1. Ding, K.; Avrutin, V.; Izyumskaya, N.; Özgür, Ü.; Morkoç, H. Micro-LEDs, a Manufacturability Perspective. *Appl. Sci.* **2019**, *9*, 1206. [[CrossRef](#)]
2. Wong, M.S.; Hwang, D.; Alhassan, A.I.; Lee, C.; Ley, R.; Nakamura, S.; Denbaars, S. High efficiency of III-nitride micro-light-emitting diodes by sidewall passivation using atomic layer deposition. *Optics Express* **2018**, *16*, 21324–21331. [[CrossRef](#)]
3. Langer, T.; Kruse, A.; Ketzer, F.A.; Schwiegel, A.; Hoffmann, L.; Jönen, H.; Bremers, H.; Rossow, U.; Hangleiter, A. Origin of the “green gap”: Increasing nonradiative recombination in indium-rich GaInN/GaN quantum well structures. *Phys. Status Solidi (c)* **2011**, *8*, 2170–2172. [[CrossRef](#)]
4. Lynsky, C.; Alhassan, A.I.; Lheureux, G.; Bonef, B.; DenBaars, S.P.; Nakamura, S.; Wu, Y.-R.; Weisbuch, C.; Speck, J.S. Barriers to carrier transport in multiple quantum well nitride-based c-plane green light emitting diodes. *Phys. Rev. Mater.* **2020**, *4*, 054604. [[CrossRef](#)]

5. Lynsky, C.; Lheureux, G.; Bonef, B.; Qwah, K.S.; White, R.C.; DenBaars, S.P.; Nakamura, S.; Wu, Y.-R.; Weisbuch, C.; Speck, J.S. Improved Vertical Carrier Transport for Green III-Nitride LEDs Using (In,Ga)N Alloy Quantum Barriers. *Phys. Rev. Appl.* **2022**, *17*, 054048. [[CrossRef](#)]
6. Pasayat, S.S.; Ley, R.; Gupta, C.; Wong, M.S.; Lynsky, C.; Wang, Y.; Gordon, M.J.; Nakamura, S.; Denbaars, S.P.; Keller, S.; et al. Color-tunable <math>10\ \mu\text{m}</math> square InGaN micro-LEDs on compliant GaN-on-porous-GaN pseudo-substrates. *Appl. Phys. Lett.* **2020**, *117*, 061105. [[CrossRef](#)]
7. White, R.C.; Li, H.; Khoury, M.; Lynsky, C.; Iza, M.; Keller, S.; Sotta, D.; Nakamura, S.; DenBaars, S.P. InGaN-Based microLED Devices Approaching 1% EQE with Red 609 nm Electroluminescence on Semi-Relaxed Substrates. *Crystals* **2021**, *11*, 1364. [[CrossRef](#)]
8. Chan, P.; Rienzi, V.; Lim, N.; Chang, H.-M.; Gordon, M.; DenBaars, S.P.; Nakamura, S. Demonstration of relaxed InGaN-based red LEDs grown with high active region temperature. *Appl. Phys. Express* **2021**, *14*, 101002. [[CrossRef](#)]
9. Jiang, F.; Zhang, J.; Xu, L.; Ding, J.; Wang, G.; Wu, X.; Wang, X.; Mo, C.; Quan, Z.; Guo, X.; et al. Efficient InGaN-based yellow-light-emitting diodes. *Photonics Res.* **2019**, *7*, 144–148.
10. Quan, Z.; Wang, L.; Zheng, C.; Liu, J.; Jiang, F. Roles of V-shaped pits on the improvement of quantum efficiency in InGaN/GaN multiple quantum well light-emitting diodes. *J. Appl. Phys.* **2014**, *116*, 183107. [[CrossRef](#)]
11. Ho, C.-H.; Speck, J.S.; Weisbuch, C.; Wu, Y.-R. Efficiency and Forward Voltage of Blue and Green Lateral LEDs with V-shaped Defects and Random Alloy Fluctuation in Quantum Wells. *Phys. Rev. Appl.* **2022**, *17*, 014033. [[CrossRef](#)]
12. Zhang, S.-N.; Zhang, J.; Gao, J.-D.; Wang, X.; Zheng, C.; Zhang, M.; Wu, X.; Xu, L.; Ding, J.; Quan, Z.; et al. Efficient emission of InGaN-based light-emitting diodes: Toward orange and red. *Photonics Res.* **2020**, *8*, 1671. [[CrossRef](#)]
13. Lynsky, C.; White, R.C.; Chow, Y.C.; Ho, W.Y.; Nakamura, S.; DenBaars, S.P.; Speck, J.S. Role of V-defect density on the performance of III-nitride green LEDs on sapphire substrates. *J. Cryst. Growth* **2021**, *560–561*, 126048. [[CrossRef](#)]
14. Wu, X.H.; Elsass, C.R.; Abare, A.C.; Mack, M.P.; Keller, S.; Petroff, P.M.; DenBaars, S.P.; Speck, J.S.; Rosner, S.J. Structural origin of V-defects and correlation with localized excitonic centers in InGaN/GaN multiple quantum wells. *Appl. Phys. Lett.* **1998**, *72*, 692–694. [[CrossRef](#)]
15. Tao, X.; Liu, J.; Zhang, J.; Mo, C.; Xu, L.; Ding, J.; Wang, G.; Wang, X.; Wu, X.; Quan, Z.; et al. Performance enhancement of yellow InGaN-based multiple-quantum-well light-emitting diodes grown on Si substrates by optimizing the InGaN/GaN superlattice interlayer. *Opt. Mater. Express* **2018**, *8*, 1221–1230. [[CrossRef](#)]
16. Jiang, X.; Zheng, C.; Mo, C.; Wang, X.; Zhang, J.; Quan, Z.; Liu, J.; Jiang, F. Study on the performance of InGaN-based green LED by designing different preparing layers. *Opt. Mater.* **2019**, *89*, 505–511. [[CrossRef](#)]
17. Zhou, S.; Liu, X.; Yan, H.; Gao, Y.; Xu, H.; Zhao, J.; Quan, Z.; Gui, C.; Liu, S. The effect of nanometre-scale V-pits on electronic and optical properties and efficiency droop of GaN-based green light-emitting diodes. *Sci. Rep.* **2018**, *8*, 1–12. [[CrossRef](#)]
18. Quan, Z.J.; Liu, J.L.; Fang, F.; Wang, G.X.; Jiang, F.Y. Effect of V-shaped Pit area ratio on quantum efficiency of blue InGaN/GaN multiple-quantum well light-emitting diodes. *Opt. Quantum Electron.* **2016**, *48*, 195. [[CrossRef](#)]
19. Wong, M.S.; Lee, C.; Myers, D.J.; Hwang, D.; Kearns, J.A.; Li, T.; Speck, J.S.; Nakamura, S.; Denbaars, S. Size-independent peak efficiency of III-nitride micro-light-emitting-diodes using chemical treatment and sidewall passivation. *Appl. Phys. Express* **2019**, *12*, 097004. [[CrossRef](#)]
20. Hwang, D.; Mughal, A.; Pynn, C.D.; Nakamura, S.; Denbaars, S. Sustained high external quantum efficiency in ultrasmall blue III-nitride micro-LEDs. *Appl. Phys. Express* **2017**, *10*, 032101. [[CrossRef](#)]
21. Qi, W.; Zhang, J.; Mo, C.; Wang, X.; Wu, X.; Quan, Z.; Wang, G.; Pan, S.; Fang, F.; Liu, J.; et al. Effects of thickness ratio of InGaN to GaN in superlattice strain relief layer on the optoelectrical properties of InGaN-based green LEDs grown on Si substrates. *J. Appl. Phys.* **2017**, *122*, 084504. [[CrossRef](#)]
22. Kusch, G.; Comish, E.J.; Loeto, K.; Hammersley, S.; Kappers, M.J.; Dawson, P.; Oliver, R.A.; Massabuau, F.C.-P. Carrier dynamics at trench defects in InGaN/GaN quantum wells revealed by time-resolved cathodoluminescence. *Nanoscale* **2021**, *14*, 402–409. [[CrossRef](#)]
23. Wu, X.; Liu, J.; Quan, Z.; Xiong, C.; Zheng, C.; Zhang, J.; Mao, Q.; Jiang, F. Electroluminescence from the sidewall quantum wells in the V-shaped pits of InGaN light emitting diodes. *Appl. Phys. Lett.* **2014**, *104*, 221101. [[CrossRef](#)]
24. Tao, T.; Zhi, T.; Liu, B.; Li, Y.; Zhuang, Z.; Xie, Z.; Chen, D.; Chen, P.; Zhang, R.; Zheng, Y. Spatially localised luminescence emission properties induced by formation of ring-shaped quasi-potential trap around V-pits in InGaN epi-layers. *Phys. Status Solidi (a)* **2014**, *211*, 2823–2827. [[CrossRef](#)]
25. Tao, X.-X.; Mo, C.-L.; Liu, J.-L.; Zhang, J.-L.; Wang, X.-L.; Wu, X.-M.; Xu, L.-Q.; Ding, J.; Wang, G.-X.; Jiang, F.-Y. Electroluminescence from the InGaN/GaN Superlattices Interlayer of Yellow LEDs with Large V-Pits Grown on Si (111). *Chin. Phys. Lett.* **2018**, *35*. [[CrossRef](#)]
26. Olivier, F.; Tirano, S.; Dupré, L.; Aventurier, B.; Largeton, C.; Templier, F. Influence of size-reduction on the performances of GaN-based micro-LEDs for display application. *J. Lumin.* **2017**, *191*, 112–116. [[CrossRef](#)]
27. Myers, D.J.; Espenlaub, A.C.; Gelzinyte, K.; Young, E.C.; Martinelli, L.; Peretti, J.; Weisbuch, C.; Speck, J.S. Evidence for trap-assisted Auger recombination in MBE grown InGaN quantum wells by electron emission spectroscopy. *Appl. Phys. Lett.* **2020**, *116*, 091102. [[CrossRef](#)]